Water vapor transport and dehydration above convective outflow during Asian monsoon

R. James,[1] M. Bonazzola,[1] B. Legras,[1] K. Surbled,[1] and S. Fueglistaler[2]

[1] We investigate the respective roles of large-scale transport and convection in determining the water vapor maximum at 100 hPa in the Asian monsoon region. The study uses backward trajectories with ECMWF ERA-Interim heating rates. It includes simple microphysics with supersaturation and takes into account convective sources based on CLAUS data with a simple parameterization of overshoots. A good agreement between reconstructed water vapor and observations is obtained over Asia. It is found that parcels belonging to the water vapor maximum have been first lifted by convection over the Bay of Bengal and the Sea of China and then transported through the tropical tropopause layer (TTL) via the monsoon anticyclonic circulation towards North-West India, where they are eventually dehydrated, avoiding the coldest temperatures of the TTL. Convective moistening accounts for about 0.3 ppmv in the Asian monsoon region and overshoots do not have a significant impact on the water vapor budget. **Citation:** James, R., M. Bonazzola, B. Legras, K. Surbled, and S. Fueglistaler (2008), Water vapor transport and dehydration above convective outflow during Asian monsoon, *Geophys. Res. Lett.*, *35*, L20810, doi:10.1029/2008GL035441.

1. Introduction

[2] The processes governing the entry of water vapor in the tropical stratosphere is debated between two hypotheses: a fast way by direct convective injection, which receives some support from observation and modelling of overshoots [*Gettelman et al.*, 2002b; *Sherwood and Dessler*, 2001; *Dessler*, 2002], and a slow way by freeze-drying at low temperature when air masses cross the tropopause under the effect of large-scale ascending motion [*Holton and Gettelman*, 2001; *Fueglistaler et al.*, 2005].

[3] In this context, the South Asian summer monsoon region is an area of particular interest, as it is characterized by a persistent maximum of water vapor extending from 150 hPa to 68 hPa [*Park et al.*, 2007], and coinciding with an ozone minimum [*Dessler and Sherwood*, 2004]. *Randel and Park* [2006] show coherent fluctuations in deep convection and water vapor inside the Asian monsoon anticyclone between the potential temperature levels 340–360 K and moistening convective events are identified in the extratropics over Asia [*Dessler and Sherwood*, 2004] and over the Tibetan Plateau [*Fu et al.*, 2006]. However, the water vapor maximum at 100 hPa does not spatially or temporally correspond to the maximum of convective activity [*Park et al.*, 2007], suggesting an important role of the horizontal transport.

[4] The upper level Asian monsoon anticyclone is known to both trap constituents in its core [*Park et al.*, 2008] and favor meridional exchanges on its flanks [*Dethof et al.*, 1999]. *Bannister et al.* [2004] and *Gettelman et al.* [2004] suggest that the moist air detrained in the TTL from convection travels around the anticyclone while rising steadily in the dynamically forced and radiatively balanced tropical upwelling. Moist air reaches into the stratosphere as it is transported southward into the deep tropics on the eastern flank of the anticyclone and bypassing coldest TTL temperatures.

[5] The aim of this study is to evaluate, exploiting new observations and new reanalysis, the respective roles of large-scale transport and convection in the formation and maintenance of the Asian monsoon water vapor maximum at 100 hPa.

2. Observations of the Asian Monsoon Region

[6] Water vapor measurements from MLS/AURA are obtained at 100 hPa from a version 2 level 2 (V2.2) product for boreal summers 2005 and 2006. As shown Figure 1 (top), a prominent water vapor maximum of 6.5 ppmv is found at 100 hPa above Asia. This anomaly is well above the precision threshold of MLS (15% according to *Livesey et al.* [2005]) and agrees with the persistent seasonal feature observed by AIRS and HALOE [*Gettelman et al.*, 2002b; *Randel and Park*, 2006]. A secondary maximum of about 5.5 ppmv corresponding to the American monsoon is observed over North Mexico and the East coast of Pacific Ocean. Figure 1 (middle) displays the zonal anomalies of PV from the ECMWF analyses at 100 hPa for the same period. The Asian monsoon anticyclone hosting the water vapor maximum appears here as a negative center of −4 PVU, extending from 30°E to 110°N and from 20°N to 40°N.

3. Method Description
3.1. Back-Trajectories Computation

[7] We compute several sets of three-dimensional backward trajectories using TRACZILLA, a modified version of the FLEXTRA model [*Stohl et al.*, 2005]. Back-trajectories are computed using reanalyses and forecasts from the ERA-INTERIM (EI) dataset. EI data are produced using cycle 29r1 of the ECMWF model and 4D-VAR assimilation [*Simmons et al.*, 2007]. They are available at T255 horizontal resolution, on 60 hybrid sigma-pressure levels.

---

[1]Laboratoire de Météorologie Dynamique, Ecole Normale Supérieure, Université Pierre and Marie Curie, CNRS, Paris, France.
[2]Department of Applied Mathematics and Theoretical Physics, University of Cambridge, Cambridge, UK.
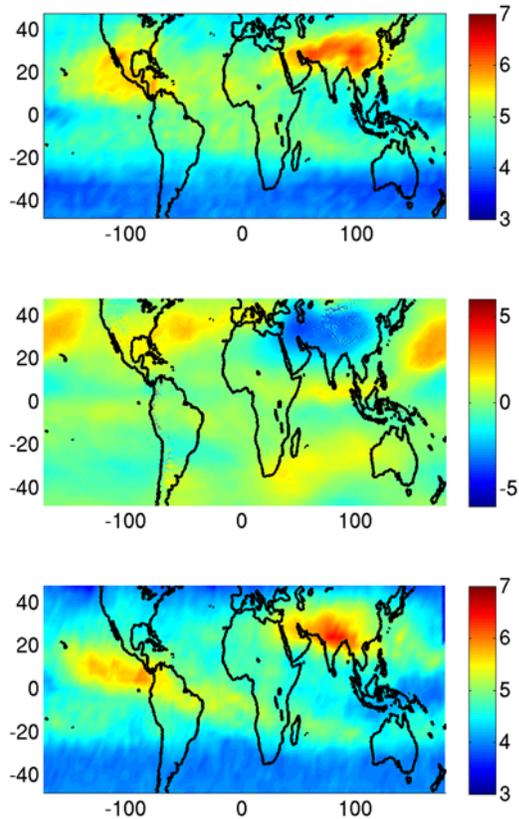
Figure 1. (top) Water vapor mixing ratio (ppmv) at 100 hPa from MLS-AURA, averaged over Jul–Aug 2005 and 2006; (middle) average potential vorticity zonal anomaly (in PVU) at 100 hPa from operational ECMWF analyses (same period); (bottom) water vapor mixing ratio at 100 hPa from back-trajectories calculations, averaged for Jul–Aug 2001, 2002, and 2003.

Meteorological variables from the EI dataset are interpolated along the trajectories.

[8] We initialize the backwards trajectories at 100 hPa, between 50°N and 50°S and at all longitudes with a horizontal spacing of $1° \times 1°$. The trajectories start weekly, during July and August, for the three years 2001, 2002 and 2003.

[9] In our reference simulation REF (described in Section 4), the trajectories are stopped if they encounter a cloud top, detected by the cloud top temperature product of the CLoud Archive User Service (CLAUS)[Hodges et al., 2000]. An intersection with a cloud is identified when the parcel experiences temperatures warmer than the local CLAUS temperature, modified by an offset of −5 K taking into account the 1–2 km underestimation of cloud top heights by thermal imagery [Sherwood et al., 2004]. If no cloud top is found along the parcel path, the trajectory is computed over 3 months.

[10] The REF trajectories are computed using 3-hourly horizontal winds and EI all-sky radiative heating rates. Since the back trajectories are stopped when they encounter their presumable convective origin, we discard the latent heat component from the total diabatic heating rates. Using heating rates instead of noisy vertical velocities strongly reduces the spurious dispersion of trajectories [Schoeberl et al., 2003].

3.2. Water Vapor Mixing Ratios Calculation

[11] Similar to previous analyses [Fueglistaler et al., 2004], we assume complete fall-out of condensate every time a cloud forms. Condensation occurs every time relative humidity exceeds $RH_{crit} = K$ 160% [Koop et al., 2000], where the coefficient K accounts for sub-grid temperature variability. The trajectories are initialized at their origin in the troposphere or stratosphere with HALOE climatological mean values depending on altitude and latitude. Those which encounter a cloud are initialized by the saturated water vapor mixing ratio at the cloud top temperature.

[12] We find best agreement with observations for $K = 0.87$, which is slightly higher than the value of $K = 0.8$ reported by Tompkins et al. [2007]. Since RH_{crit} depends mainly on the temperature, moisture is controlled by the minimum temperature along the trajectory. We found that the summer EI temperature in the TTL is about 0.7 K colder than in the ERA-40, a feature that would yield a dry bias if condensation is assumed at $RH = 100\%$ as done by Fueglistaler et al. [2004] for ERA-40.

4. Results of the Reference Simulation

[13] Figure 1 (bottom) shows the water vapor field at 100 hPa inferred from REF back-trajectory calculations. Comparison with Figure 1 (top) shows that the patterns and the absolute values of MLS measurements are retrieved by our reconstruction. The Asian monsoon water vapor maximum is reproduced with a mean mixing ratio of 6.5 ppmv extending from Iraq to China Sea and from Central India to North Tibet. The water vapor mixing ratios are also retrieved reasonably well over the Oceania minimum and the winter subtropical barrier. The American monsoon maximum is recovered but displaced to the south.

[14] To determine the regions where the air parcels ending up at 100 hPa were lifted by convection, we display in Figure 2 the distribution of the intersections of the back-trajectories with the cloud tops. Figure 2a shows that 60% of the parcels originate from convective sources located over the north–west coast of the Bay of Bengal and South China sea, whereas small contributions are found from Indonesia, the American monsoon region and the Guinean Gulf. Our results using CLAUS yield much more localised convective sources than those of Fueglistaler et al. [2005], and little contribution from the Tibetan plateau. Figure 2c displays the probability density functions (PDF) of convective sources levels and dehydration levels, expressed in potential temperatures, and shows very little overlap between these two distributions. This result points out that, although most of the parcels are lifted up to 360 K by intense convection, they are advected afterwards by large-scale transport across the TTL temperatures that eventually control the water vapor entry in the lower stratosphere. The overall description is in agreement with OLR observations and corroborates the large-scale transport hypothesis suggested by [Park et al., 2007].

[15] To analyze further the mechanisms of formation and maintenance of the Asian monsoon water vapor maximum, we consider the locations of the Lagrangian temperature
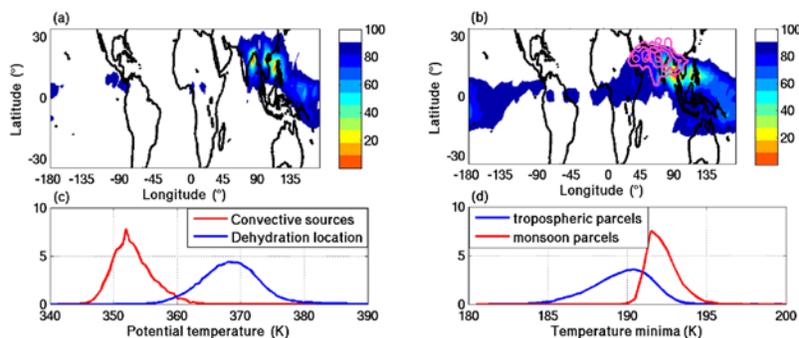
Figure 2. (a) Distribution of intersections of back-trajectories with cloud tops from CLAUS. (b) Distribution of the locations where the Tropospheric parcels have encountered their temperature minima. Distributions in Figures 2a and 2b are calculated by binning parcels within boxes of $1° \times 1°$. Colors show isodensity and the color scale shows cumulated percentage of parcels (inside each color domain) obtained by aggregating boxes starting from the most populated. Red contours in Figure 2b show the distribution for the Monsoon parcels. (c) PDF of the altitudes (in potential temperature) where parcels cross clouds tops (red) and where they are dehydrated (blue); (d) PDFs of the Lagrangian temperature minima for the Tropospheric (blue) and the Monsoon (red) ensembles.

minima for two ensembles of back-trajectories. The "Tropospheric ensemble" is composed of back-trajectories which experienced potential temperatures lower than 350 K at least once during the simulation. The "Monsoon Ensemble" is composed of trajectories initialized over Asia ($35–120°E$ and $25–40°N$) and associated with water vapor mixing ratios greater than 5 ppmv at 100 hPa.

[16] Figure 2b shows that 75% of the parcels of the Tropospheric Ensemble experience their Lagrangian temperature minima in the coldest regions of the Bay of Bengal, China Sea and Micronesia, in the vicinity of the convective sources. On the other hand, the temperature minima of the Monsoon parcels are on average 2.3 K warmer than for the Tropospheric ensemble (Figure 2d), and are located over the North of the Bay of Bengal, North–West India and Saudi Arabia. This does not contradict the cold point temperature minimum found by *Schmidt et al.* [2004] over the monsoon region because it occurs above 100 hPa and is thus not sampled by our back-trajectories. The warm bias can explain an increase of 1.5 ppmv in water vapor mixing ratio. Hence, the Monsoon parcels are transported North–

Westward from the convective sources by the anticyclonic circulation during their slow ascent, avoiding the coldest regions of the TTL and remaining moister than average Tropospheric parcels. Our scenario explaining the moisture anomaly at 100 hPa in the Asian Monsoon region is consistent with the results of *Bannister et al.* [2004], although their simulations show a water vapor maximum located over China Sea rather than North India.

5. Discussion and Conclusion

[17] It is important to test the sensivity of our results to the assumptions and parameterizations used above. Best results are obtained when supersaturation of 140% is allowed (with $K = 0.87$). Removing supersaturation induces a $0.8–1.6$ ppmv dry bias over the tropics (not shown). Moistening can be obtained by other microphysical processes than supersaturation, like for example evaporation of ice crystals, not included in our model. However the results of *Bonazzola and Haynes* [2004] based on the model of *Gettelman et al.* [2002a] indicate that these processes are
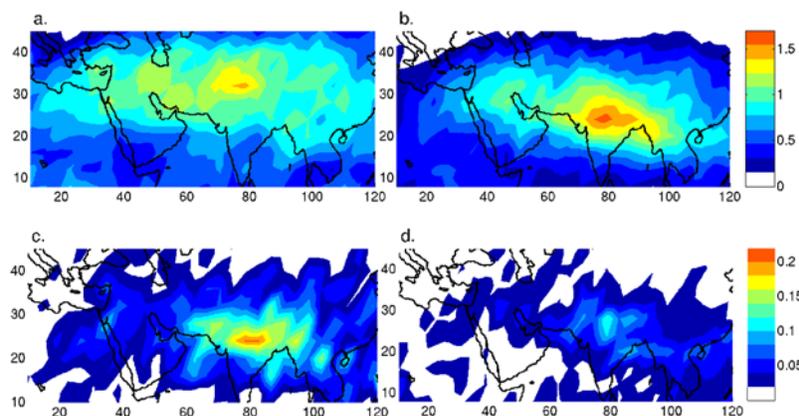

Figure 3. (a) Difference, in calculated water vapor mixing ratio (ppmv), between REF and the simulation performed with vertical winds. (b) Difference between REF and the simulation performed with clear-sky heating rates. (c) Difference between REF and the simulation ignoring cloud tops. (d) Difference between the simulation including overshoots and REF.

secondary and supersaturation, on the other hand, is an important process that must be included in large-scale models [*Tompkins et al.*, 2007].

[18] Figure 3 compares REF simulation with several sensivity experiments. Figure 3a shows the difference between REF and a simulation using standard vertical velocities instead of heating rates. Water vapor decreases by 1 ppmv in the Asian monsoon region and by 0.8 ppmv in the Southern hemisphere subtropics, showing that all-sky radiative heating rates are essential to reproduce observations. *Immler et al.* [2007] reached the same conclusion in order to simulate tropical cirrus. Here, the noise in the vertical wind fields leads to an enhanced dispersion of parcels provoking a decrease of Lagrangian temperature minima.

[19] Figure 3b compares REF with a simulation where heating rates are reduced to the clear sky component. In this simulation, the back-trajectories are never able to reach isentropic levels below 360 K and are trapped in the cold levels of the TTL, resulting into much too dry air at 100 hPa. This indicates that the vertical transport in the TTL is strongly influenced by the radiative effect of clouds.

[20] Figure 3c compares REF with a simulation where trajectories are all run for three months and are not stopped by the intersection with clouds. The parcels affected by this modification have longer trajectories, along which they can experience colder temperatures. The difference in water vapor mixing ratio can be interpreted as an effect of moistening by convective detrainment. Note, however, that large-scale motion is also affected by the location of convective events, and that this effect cannot be discarded in the sensitivity experiment. Differences are largest (0.3 ppmv) in the Asian region of deep convection, but are still low compared to the absolute values of the mixing ratios there. We thus identify pure large-scale transport, rather than convective transport, as the most important component controlling the water vapor budget at 100 hPa.

[21] Figure 3d compares REF with a simulation that adds a representation of convective overshoots. We consider here that there is a chance for a parcel to be detrained above the convective decks detected from corrected CLAUS temperature. The probability is set to one at cloud top and decreases exponentially with height. Consistently with [*Liu and Zipser*, 2005], the probability is set, respectively, to 0.6% and 1.5% above sea and land, for a difference in temperature between the parcel and the cloud top corresponding to a distance of 1 km, depending on the local lapse rate. The comparison shows almost no impact on the water vapor mixing ratio. The occurrence of overshoots needs to be unrealistically 100 times more frequent than estimated by [*Liu and Zipser*, 2005] to increase the water vapor mixing ratio by 0.3 ppmv on a global mean over the tropics. Our interpretation is that large-scale transport leads to a high probability that overshooting parcels encounter temperatures below saturation temperatures, thus 'erasing' much of the imprint of convection [*Dessler et al.*, 2007].

[22] The main result of this work is to show that the observed maximum of water vapor mixing ratio at 100 hPa within the Asian monsoon anticyclone can be explained by the effect of large-scale advection which translates the crossing of the tropopause to warmer region than just above

most active convection. It is shown that the direct moistening by overshooting convection plays a minor role although this conclusion does not necessarily hold for other seasons and other regions.

References

Bannister, R. N., A. O'Neill, A. R. Gregory, and K. M. Nissen (2004), The role of the south-east Asian monsoon and other seasonal features in creating the 'tape-recorder' signal in the Unified Model, *Q. J. R. Meteorol. Soc.*, *130*, 1531–1554.

Bonazzola, M., and P. H. Haynes (2004), A trajectory-based study of the tropical tropopause region, *J. Geophys. Res.*, *109*, D20112, doi:10.1029/2003JD004356.

Dessler, A. E. (2002), The effect of deep, tropical convection on the tropical tropopause layer, *J. Geophys. Res.*, *107*(D3), 4033, doi:10.1029/2001JD000511.

Dessler, A. E., and S. C. Sherwood (2004), Effect of convection on the summertime extratropical lower stratosphere, *J. Geophys. Res.*, *109*, D23301, doi:10.1029/2004JD005209.

Dessler, A. E., T. F. Hanisco, and S. Fueglistaler (2007), Effects of convective ice lofting on H_2O and HDO in the tropical tropopause layer, *J. Geophys. Res.*, *112*, D18309, doi:10.1029/2007JD008609.

Dethof, A., A. O'Neill, and J. M. Slingo (1999), A mechanism for moistening the lower stratosphere involving the Asian summer monsoon, *Q. J. R. Meteorol. Soc.*, *125*, 1079–1106.

Fu, R., Y. Hu, J. S. Wright, J. H. Jiang, R. E. Dickinson, M. Chen, M. Filipiak, W. G. Read, J. W. Waters, and D. L. Wu (2006), Short circuit of water vapor and polluted air to the global stratosphere by convective transport over the Tibetan Plateau, *Proc. Natl. Acad. Sci. U. S. A.*, *103*(15), 5664–5669.

Fueglistaler, S., H. Wernli, and T. Peter (2004), Tropical troposphere-to-stratosphere transport inferred from trajectory calculations, *J. Geophys. Res.*, *109*, D03108, doi:10.1029/2003JD004069.

Fueglistaler, S., M. Bonazzola, P. H. Haynes, and T. Peter (2005), Stratospheric water vapor predicted from the Lagrangian temperature history of air entering the stratosphere in the tropics, *J. Geophys. Res.*, *110*, D08107, doi:10.1029/2004JD005516.

Gettelman, A., W. J. Randel, F. Wu, and S. T. Massie (2002a), Transport of water vapor in the tropical tropopause layer, *Geophys. Res. Lett.*, *29*(1), 1009, doi:10.1029/2001GL013818.

Gettelman, A., M. L. Salby, and F. Sassi (2002b), Distribution and influence of convection in the tropical tropopause region, *J. Geophys. Res.*, *107*(D10), 4080, doi:10.1029/2001JD001048.

Gettelman, A., D. E. Kinnison, T. J. Dunkerton, and G. P. Brasseur (2004), Impact of monsoon circulations on the upper troposphere and lower stratosphere, *J. Geophys. Res.*, *109*, D22101, doi:10.1029/2004JD004878.

Hodges, K., D. W. Chappell, G. J. Robinson, and G. Yang (2000), An improved algorithm for generating global window brightness temperatures from multiple satellite infra-red imagery, *J. Atmos. Oceanic Technol.*, *17*, 1296–1312.

Holton, J. R., and A. Gettelman (2001), Horizontal transport and the dehydration of the stratosphere, *Geophys. Res. Lett.*, *28*, 2799–2802.

Immler, F., K. Krüger, S. Tegtmeier, M. Fujiwara, P. Fortuin, G. Verver, and O. Schrems (2007), Cirrus clouds, humidity, and dehydration in the tropical tropopause layer observed at Paramaribo, Suriname (5.8°N, 55.2°W), *J. Geophys. Res.*, *112*, D03209, doi:10.1029/2006JD007440.

Koop, T., B. P. Luo, A. Tsias, and T. Peter (2000), Water activity as the determinant for homogeneous ice nucleation in aqueous solutions, *Nature*, *406*, 611–614.

Liu, C., and E. J. Zipser (2005), Global distribution of convection penetrating the tropical tropopause, *J. Geophys. Res.*, *110*, D23104, doi:10.1029/2005JD006063.

Livesey, N. J., et al. (2005), EOS MLS version 1.5 Level 2 data quality and description document, *JPL Publ.*, *D-32381*.

Park, M., W. J. Randel, A. Gettelman, S. T. Massie, and J. H. Jiang (2007), Transport above the Asian summer monsoon anticyclone inferred from Aura Microwave Limb Sounder tracers, *J. Geophys. Res.*, *112*, D16309, doi:10.1029/2006JD008294.

Park, M., W. J. Randel, L. K. Emmons, P. F. Bernath, K. A. Walker, and C. D. Boone (2008), Chemical isolation in the Asian monsoon anticyclone observed in Atmospheric Chemistry Experiment (ACE-FTS) data, *Atmos. Chem. Phys.*, *8*, 757–764.

Randel, W. J., and M. Park (2006), Deep convective influence on the Asian summer monsoon anticyclone and associated tracer variability observed with Atmospheric Infrared Sounder (AIRS), *J. Geophys. Res.*, *111*, D12314, doi:10.1029/2005JD006490.

Schmidt, T., J. Wickert, G. Beyerle, and C. Reigber (2004), Tropical tropopause parameters derived from GPS radio occultation measurements with CHAMP, *J. Geophys. Res.*, *109*, D13105, doi:10.1029/2004JD004566.

Schoeberl, M. R., A. R. Douglass, Z. Zhu, and S. Pawson (2003), A comparison of the lower stratospheric age spectra derived from a general circulation model and two data assimilation systems, *J. Geophys. Res.*, *108*(D3), 4113, doi:10.1029/2002JD002652.

Sherwood, S. C., and A. E. Dessler (2001), A model for transport across the tropical tropopause, *J. Atmos. Sci.*, *58*, 765–779.

Sherwood, S. C., J.-H. Chae, P. Minnis, and M. McGill (2004), Underestimation of deep convective cloud tops by thermal imagery, *Geophys. Res. Lett.*, *31*, L11102, doi:10.1029/2004GL019699.

Simmons, A., S. Uppala, D. Dee, and S. Kobayashi (2007), ERA-Interim: New ECMWF reanalysis products from 1989 onwards, *ECMWF Newsl.*, *110*, 29–35.

Stohl, A., C. Forster, A. Frank, and G. Wotawa (2005), Technical note: The Lagrangian particle dispersion model FLEXPART version 6.2, *Atmos. Chem. Phys.*, *6*, 2461–2474.

Tompkins, A. M., K. Gierens, and G. Rädel (2007), Ice supersaturation in the ECMWF integrated forecast system, *Q. J. R. Meteorol. Soc.*, *133*, 53–63.

_____

M. Bonazzola, Laboratoire de Météorologie Dynamique, Ecole Normale Supérieure, Université Pierre et Marie Curie, CNRS, 4 place Jussieu, Tour 45–55, 3eme étage case postale 99, F-75252 Paris CEDEX 05, France.

S. Fueglistaler, Department of Applied Mathematics and Theoretical Physics, University of Cambridge, Centre for Mathematical Sciences, Wilberforce Road, Cambridge CB3 0WA, UK.

R. James, B. Legras, and K. Surbled, Laboratoire de Météorologie Dynamique, Ecole Normale Supérieure, Université Pierre et Marie Curie, CNRS, 24 rue Lhomond, F-75005 Paris CEDEX 05, France. (james@lmd.ens.fr)